Composite Materials
2022; 6(2): 49-58
http://www.sciencepublishinggroup.com/j/cm
doi: 10.11648/j.cm.20220602.11

Analysis of Damage-Induced on Fiber Reinforced S-Glass Composite Laminate at Low Velocity Loading Condition

Enock Andrews Duodu

Department of Mechanical and Automotive Technology Education, Akenten Appiah-Menka University of Skills Training and Entrepreneurial Development, Kumasi, Ghana

Email address:
eaduodu@aamusted.edu.gh

To cite this article:
Enock Andrews Duodu. Analysis of Damage-Induced on Fiber Reinforced S-Glass Composite Laminate at Low Velocity Loading Condition. *Composite Materials*. Vol. 6, No. 2, 2022, pp. 49-58. doi: 10.11648/j.cm.20220602.11

Received: September 14, 2022; **Accepted**: October 14, 2022; **Published**: October 29, 2022

Abstract: Structural performance of reinforced S-glass composite laminate at low velocity impact loading was investigated with three different impactors to characterize the induced-damage behavior. In this study, a total of 12 samples were tested numerically with three distinct impactors at four different energy thresholds 5-13 J to examine the damage behavior of the reinforced S-glass composite laminate in terms of intra-laminar, inter-laminar and stress failure responses. Dynamic finite element coded ABAQUS/Explicit software through user-written subroutines was used to create the geometry models to capture the impact damage response. A composite laminate plate of diameter 150 mm and thickness 6.5 mm with stacking configuration $[90/45/45/0/-45]_S$ was designed together with three different impactor geometrical shapes (spherical, flat cylindrical and conical). The flat cylindrical impactor measures 15 mm radius and 20 mm high; the conical shape length 20 mm, radius 15 mm with a tip-end angle of 112°; while the spherical impactor measures 15 mm in radius. This impactor was modeled as analytical rigid body of mass 1.6 kg with a force of 15.69 N prescribed in transverse direction and composite plate was actuated by surface-to-surface contact pairs within ABAQUS/Explicit platform with penalty enforcement contact method. A relative fine element mesh of 0.1 mm x 0.1 mm was applied on the impact location on the composite laminate with failed interface elements allowed to remain in the model to circumvent penetration of damage layers using an element option platform. A total number of 83640 solid elements, 75276 cohesive elements and 171420 nodes were applied for the simulation. This study discloses that irrespective of impactor profile, damage threshold increases with increase in impact energy level. The dominant damage modes found in the composite laminate are matrix cracking and delamination. The study also shows better correlation among the models for damage area responses and that flat head impactor exhibits largest delamination area compared to spherical and conical edge impactors. The study shows that stress value on the conical edge impactor is greater on the impacted layer and lesser on the bottom layer amongst the impactors due to geometrical profile. Comparison amongst the models raises the necessity to incorporate energy distortion criterion into this constitutive damage model. It is therefore recommended to engineers and researchers to adapt this model to improve and optimize the design processes of composite materials in the automobile and aviation structural applications.

Keywords: Damage-Induced, Delamination, Impactors, Stress Distribution, User-Defined Material

1. Introduction

The extensive used of composite laminates for structural applications are increasing in the area of aviation industry due to their superior material properties. However, composite laminates are typically poor to resist impact damage. This limitation has become serious design issue and tends to constrain the structural application of this material in the aeronautics and astronautics industry which requires high damage resistance. Composite laminates failure is a complex process which encompasses intra-laminar and inter-laminar damages resulting in loss of stiffness and load-carrying ability as damage threshold becomes enormous. In practice, intra-laminar damage occurs in the form of matrix compression and tension damage, fiber-matrix debonding; and at high loading condition where compressive and tensile fiber breakage mode occur eventually leading to ultimate failure of the composite laminates. Matrix cracking and splitting along the fiber direction is established as the initial damage element occurring in transverse loading direction as a result of dominance of resin behavior. In low velocity impact loading,

delamination is believe to be the main damage mode of the composite laminate causing palpable material properties degradation due to stress concentration between inter-laminar plies. Structural components in aircraft made of composite proves to be susceptible to impact loading, therefore, different aspects of damage behavior of composite laminates are under scrutiny for efficient modelling analysis.

Several studies in reference through experimental tests [1-4] analytical formulations [5-10] and finite element methods [11-16] have been documented on reinforced composite laminates. Evci and Gulgec [17] used experimental study to performed investigation on impact behavior of three composite laminates with low-velocity impact loadings where result shows that strength and stiffness in unidirectional E-glass laminate is less as compared to woven E-glass and aramid laminates; and that large damage area is envisaged in the unidirectional composite than in the woven E-glass and aramid laminates. Result also reveals better shock absorbing capacity in woven E-glass than the other laminates under dynamic loading condition but low in static loading. Yang, et al. [18] have conducted numerical simulation to predict impact behavior of fiber reinforced composite laminate under low velocity. It found that matrix cracking evolve as the first damage envelop and occurs in the last layer of the composite plate, followed by delamination, fiber pull-out and fiber breakage. Also, Panettire et al. [19] carried out low velocity numerical analysis with empirical validation to determine realistic impact energy level on quasi-isotropic composite laminate. Result shows that low energy level produces large amount of oscillatory force for delamination; however, ultrasonic scans did not reveal any internal damage resulting in unfavorable effects of the dissipation mechanisms of the impactor. Mishra et al. [20] have used analytical method to assess the impact behavior of rectangular E-glass/epoxy composites (cross-ply and woven fabric) under low-velocity. The result shows that cross-ply composite laminates are less resistant to impact damage than woven fabric composite. Lopresto and Caprino [21] have carried out analytical study via the exponent power law to establish damage response of composite laminates under low-velocity. The study found that inter-laminar damage increase with increase in laminates thickness. Similarly, Harpreet and Mahajan [22] used analytical formulation to estimate the impact deformation in composite laminate under low-velocity. It found that the model is capable to estimate damage extension envelop around the impact zone which agrees well with experimental and numerical results. Farooq and Myler [23] have numerically establish computational model to predict the failure behavior of thick carbon fiber reinforced composite plates subjected to low-velocity with round-and- flat impactors. The model is capable to predict ply and ply-ply damage which correlated better with experimental observation. It found that intra- and inter-damages of the round-nose impactor is slightly less than the flat-nose impactor.

More recently, Topac et al. [24] have carried out a 3D-numerical analysis and through experimental test validation on carbon fiber reinforced plastics laminate plate to examine the damage behavior at low velocity. Computational results show good accord with real-time experimental observation in terms of interface delamination and ply failure. Sakly et al [25] developed a commercial finite element model to assess the damage response in sandwich composite laminates with low-velocity impact. Numerical simulation result shows that impact wave evolution is localized within the impact zone when compared with empirical test. Lopes et al. [26] carried-out simulation studies to evaluate the failure behavior in unidirectional composite laminate under low velocity impact. This model provides a dent on the impacted surface which makes its reliable to predict inter-laminar and intra-laminar damages above and below the BVID impact energy regimes. Similarly, Perez et al. [27] have formulated a numerical model to predict the internal induced deformation in quasi-isotropic composite laminate at low-velocity impact. Result showed that the model is dependable to predict intra-laminar damage as well as crack initiation and growth without the establishment of cohesive interfaces; and in good collaboration with observation test. Alshahrani et al. [28] have presented a 3D finite element model of low-velocity impact to estimate the performance of glass fiber/epoxy composite laminate. Simulation results showed that matrix cracking and delamination damage mostly occur first in low-velocity failure assessment followed by fiber breaking, which agrees well with experimental validation test. Bienias et al. [29, 30] have presented a numerical model using the finite element ABAQUS via user-defined subroutine to evaluate the damage response in fiber metal laminates under low-velocity loading. Results confirm that the model response is in good agreement with empirical test in terms of inter-and intra-damages.

Many referenced studies [31-34] stated that composite laminate damage initiation correspond to impactor head profile. As remarked above, most of the studies employed either the round nose, flat cylindrical or spherical impactors for impact damage analysis. The effect of rigid conical edge impactor is not much studied. Therefore, the present study introduces a novel conical edge impactor for structural damage evaluation and compares to both spherical and flat cylindrical impact loading conditions. The study seeks to develop a model capable to trigger crack initial response and ultimate failure of reinforced S-glass composite laminate in aircraft structures. The aim of this study is to investigation the low velocity impact behavior of aviation S-glass fiber reinforced composite laminate through finite element method. Numerical results obtained from the models are compared among the three impactors at four different energy levels ranging from 5 to 13 J.

2. Model Formulations

2.1. Intra-Laminar Damage

In the study, intra-laminar damage is envisaged to occur and therefore constitutive laws are required to trigger damage initiation and propagation. The failure modes are developed and executed in ABAQUS/Explicit solver through the user-defined material subroutine. Hence, 3D Hashin failure criterion in

reference [35] is adopted and adapted to simulate intra-layer fiber and matrix failures, and described in Eqs. (1-4) as follow:

Matrix tension failure

$$\left(\frac{\sigma_{22}}{Y_t}\right)^2+\left(\frac{\tau_{12}}{S_t}\right)^2=1 \quad (1)$$

Matrix compression failure

$$\left(\frac{\sigma_{22}}{2S_t}\right)^2+\left[\left(\frac{Y_t}{2S_t}\right)^2-1\right]\left(\frac{\sigma_{22}}{Y_t}\right)^2+\left(\frac{\tau_{12}}{S_l}\right)^2=1 \quad (2)$$

Fiber tension failure

$$\left(\frac{\sigma_{11}}{X_t}\right)^2+\alpha\left(\frac{\tau_{12}}{S_l}\right)^2=1 \quad (3)$$

Fiber compression failure

$$\left(\frac{\sigma_{11}}{X_c}\right)^2=1 \quad (4)$$

where σ_{11} and σ_{22} are the normal stress in fiber and transverse directions, respectively. τ_{12} shows shear stress in fiber and transverse in-plane directions. X_c and X_t represent the fiber compressive and tensile strengths, Y_t is the matrix compressive strength, S_t and S_l denote allowable shear strength in transverse direction and shear strength in fiber and transverse plane. α is the material property coefficient that account for shear stress contribution in the fiber tensile failure mode.

2.2. Inter-Laminar Damage

Inter-laminar damage in stiffened composite panel is very complex phenomenon during initiation and growth regimes; therefore cohesive zone model is established via integrated mixed-mode criterion to stimulate the damage initiation threshold. A cohesive interface model based on quadratic strain interaction criterion (Eq. 5) is employed as defined in reference [36].

$$\left(\frac{\langle\delta_n\rangle}{\delta_n^0}\right)^2+\left(\frac{\delta_s}{\delta_s^0}\right)^2+\left(\frac{\delta_t}{\delta_t^0}\right)^2\geq 1 \quad (5)$$

δ_n^0, δ_s^0 and δ_t^0 denote the normal and shear direction of contact separation peak values, with corresponding δ_n, δ_s and δ_t separation mode displacements. To describe the normal and shear separation damage evolution along the interface, an effective separation δ_m is incorporated into the model as expressed in Eq. (6);

$$\delta_m=\sqrt{\langle\delta_n\rangle^2+\delta_s^2+\delta_t^2} \quad (6)$$

Delamination growth under mixed mode loading based on B-K energy fracture criterion detailed in reference [36] is used.

$$G^c=G_n^c+\left(G_s^c-G_n^c\right)\left(\frac{G_s^c+G_t^c}{G_s^c+G_n^c}\right)^\eta \quad (7)$$

The normal and shear critical fracture energy in Eq. 7 is represented by G_n^c, G_s^c and G_t^c, respectively, G^c denotes fracture energy of delamination, with η as cohesive coefficient.

FORTRAN pre-compiler code involving these constraint equations is written and executed into the commercial explicit finite element software ABAQUS 6.11 version through a user-coded material subroutine [37].

3. Numerical Application

3.1. Geometrical Model and Boundary Conditions

Dynamic finite element ABAQUS/Explicit package is employed to create the geometry models (Figure 1) of reinforced S-glass fiber/epoxy composite laminate to capture the impact damage response. In the simulation, three different impactor geometrical shapes (spherical, flat cylindrical and conical) are used. The flat cylindrical impactor measures 15 mm radius and 20 mm high; the conical shape length 20 mm, radius 15 mm with a tip-end angle of 112°; while the spherical impactor measures 15 mm in radius. A fiber reinforced S-glass composite laminate plate of diameter 150 mm and thickness 6.5 mm with stacking configuration $[90/45/45/0/-45]_S$ is designed. The impactor is modeled as analytical rigid body of mass 1.6 kg with a force of 15.69 N prescribed in transverse direction. Different initial impact velocities are specified to the impactor to actuate different impact energy portfolios in the range of 5-13 J. Constrained boundary conditions are fully apportioned along the circumference of the composite plate, with all DOFs restrained to zero to mimic experimental setup as shown in Figure 1.

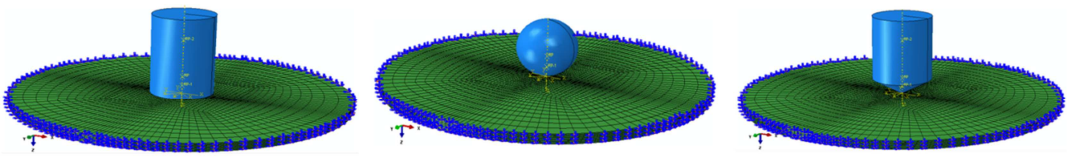

(a) (b) (c)

Figure 1. *Assembled finite element models with boundary conditions (a) flat cylindrical impactor (b) spherical impactor (c) conical edge impactor.*

3.2. Element Used and Mesh Density

In addition to the eight nodes, three point integration linear brick elements (C3D8R) with reduced integration used to model the composite laminate, traction separation cohesive elements (COH3D8) of zero-thickness are introduced between layers with different ply configurations to discretize the interface for debonding activation. The quadratic strain interaction criterion and B-K energy fracture law are used to predict damage initiation and propagation, whiles stress-based 3D Hashin failure criterion is adopted for intra-laminar damage together with a continuum damage mechanics available in ABAQUS/Explicit software. A relative fine element mesh of 0.1 mm x 0.1 mm is applied on the impact location on the stiffener. Failed interface elements were allowed to remain in the model to circumvent penetration of damage layers using an element option in ABAQUS/Explicit platform. A total number of 83640 solid elements, 75276 cohesive elements and 171420 nodes were applied for the simulation.

3.3. Contact and Material Properties

The interaction between the analytical rigid impactor and composite plate is actuated by surface-to-surface contact pairs within ABAQUS/Explicit platform with penalty enforcement contact method [38], and this is applied to avoid arbitrary penetration. The material properties and cohesive parameters obtained from literature [39, 40] are listed in Table 1.

3.4. Computational Procedure

The formulated constitutive model is executed in the material user subroutine compiled in FORTRAN, and linked with the commercial finite element solver in ABAQUS/Explicit. Figure 2 shows the computational flow process of the model. Throughout the computational process, ABAQUS/Explicit transfers information of strain increment to the subroutine (material properties, strain increment of the current increment step, time increment size as well as the state variables of the previous increment step such as strain and damage). When the material variables are entered and the failure benchmark is fulfilled, the homogenized-material properties reduction is performed to update the failed variables. The stresses/strains at the integration points of the elements are updated by the reduced stiffness matrix. The updated variables returned to ABAQUS/Explicit for next step of analysis to commence.

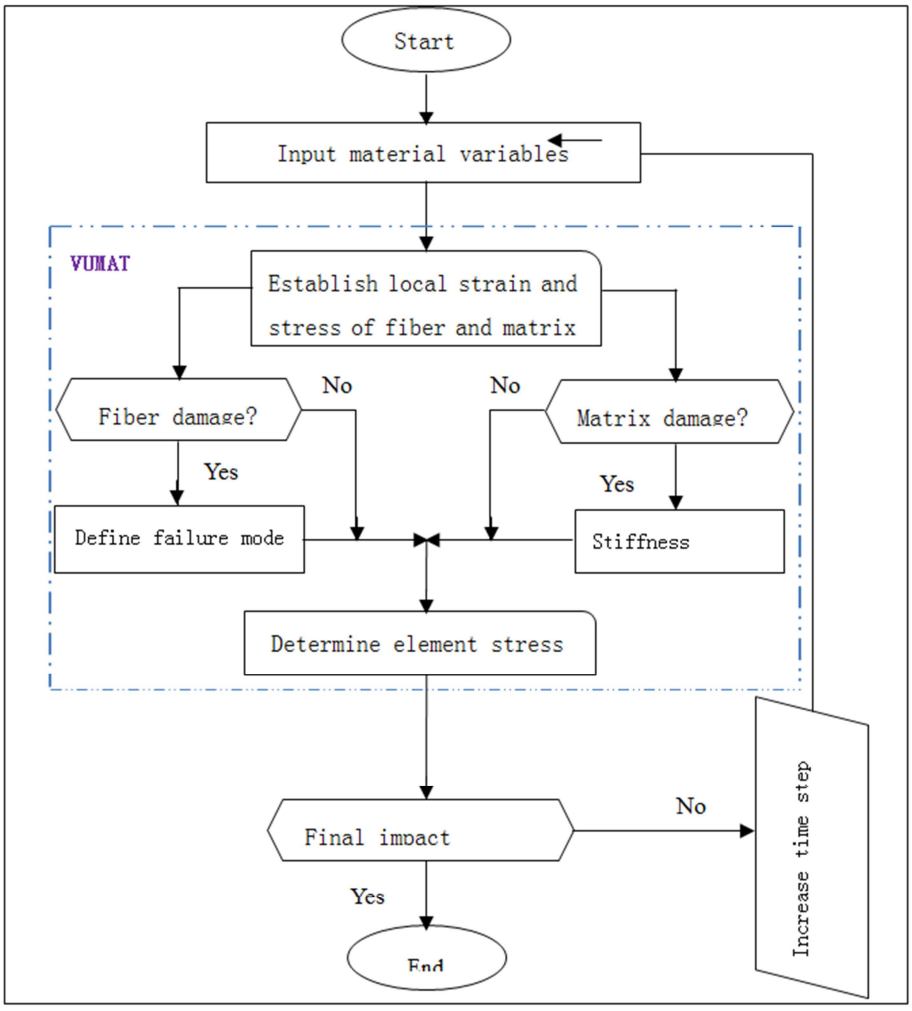

Figure 2. *Flow diagram of computational impact process.*

Table 1. *Material properties and cohesive parameters used in the model analysis.*

Density		**1800 kg/m^3**
Laminate	Elastic properties	E_{11} = 40 GPa; E_{22} = E_{33} = 13 GPa; ν_{12} = ν_{13} = 0.057; ν_{23} = 0.36 G_{12} = G_{13} = 3.15 GPa; G_{23} = 4.7 GPa
	Strength	X_t = 0.98 GPa; X_c = 10 GPa; Y_t = 0.044 GPa; Y_c = 0.285 GPa; Z_t = 0.044 GPa; Z_c = 0.285 GPa; S_{12} = 0.0606 MPa; S_{13} = 0.0606 GPa; S_{23} = 0.022 GPa; a= 2
Cohesive element	Elastic properties	$K_n = 4.16\times10^6$; $K_s = K_t = 7.041\times10^3$ N/mm^3
	Strength	δ_n^0 = 60 MPa; $\delta_s^0 = \delta_t^0$ = 90 MPa
	Fracture energy	G_{IC} = 1200 N/m^2; $G_{IIC} = G_{IIIC}$ = 3000 N/m^2; η = 2

4. Results and Discussion

Computational images were compared with that of experimental test for validation. A total of 12 samples were tested numerically with the three distinct impactors at four different energy thresholds to examine the damage behavior of the reinforced S-glass composite laminate. In this model, impact behavior was also analyzed in terms of intra-laminar, inter-laminar and stress failure responses.

4.1. Validation of Composite Laminate

An experimental test [32] C-scan images were used to validate the damage model. Accordingly, impact damage induced by flat head impactor was compared to the simulated damage on the impact surface of the composite laminate at four impact energy levels as shown in Figure 3. Flat headed impactor was considered as one of the common damage regimes in aviation industry, hence applied for validation. It can be seen from the images that reasonable difference is established in the damage shape caused by the flat head impactor, even at higher impact energy threshold. As shown (Figure 3), the flat head occupied a large contact space resulted in internal deformation due to small concentration on the impacted surface. It can be observed that apart from the lower energy threshold where damage shape matches well with the C-scan images, the other impact energy levels predicted damage shape dotted around the impact zone. The discrepancy between the test images and simulation images may perhaps occur due to approximation in the damage model.

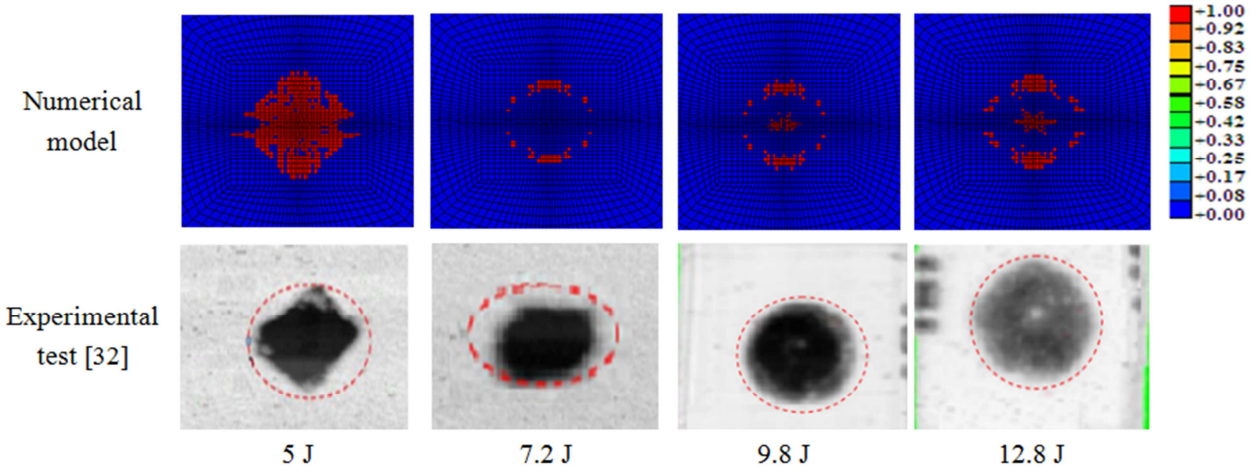

Figure 3. *Validation of the model with flat cylindrical impactor at different impact energy levels.*

4.2. Damage Induced Analysis of Composite Laminate

4.2.1. Comparison of Inter-Laminar Damage with Different Impactors

Figure 4 shows delamination area on the inter-laminar interface-1 for the three impactors under different impact energy levels. It can be seen from the images that the largest delamination is visualized using the flat cylindrical impactor followed by the spherical impactor. Result also shows that delamination damage on the interface is almost equal at all impact energy levels with regards to the flat cylindrical impactor. On the contrary, delamination shapes via the other impactors predicted growing damage when energy threshold increases. Using the spherical impactor to activate interlaminar damage on the 1st interface, an asteroid damage pattern is formed. It is observed however, that delamiantion is considerably larger during impact energy threshold in the 12.8 J followed by 7.2 J with least damage area prediction under the 5 J impact energy threshold. In a similar accord, an asteriod damage envelop is numerically formed on all the impact events using the conical edge impactor. Here, this type of impactor exhibited massive damage during the 12.8 J regime with smallest damage shape predicted during the 7.2 J energy threshold.

Additionally, delamination shape of selected interfaces with different impactors under 7.2 J impact energy level is presented in Figure 5. It is observed once again that damage portfolio via the flat headed impactor generated the lagest

damage among the impactors to show the effect of impactor geometry on damage development as confirmed in literature [41]. As can be seen, though, the damage shapes are similar, the 9th interface exhibited deep and massive damage compared to interface-3 and interface-6. This damage phenomenon could be attributed to long contact duration between the impactor and bottom layer resulted in flexural deformation and transverse shear stresses leading to delamination. Based on Figures 4 and 5, results comprehended that damage threshold is not only governed by impactor geometry but also influenced by impact energy levels. This attests to the fact that delamination is believed to be the main damage mode in composite laminate causing palpable material properties degradation due to stress concentration between inter-laminar plies, which collaborated well with reference [42]. Moreover, delamination is assumed to be instigated by intralaminar damage in terms of matrix cracking and fiber breaking as well as transverse shear stresses. It is also noted however, that among the impactors, the flat head profile exhibited largest delamination area which is in agreement with Ref. [32]. This phenomenon confirmed that damage area caused by the spherical and conical edge impactors are more localized [31].

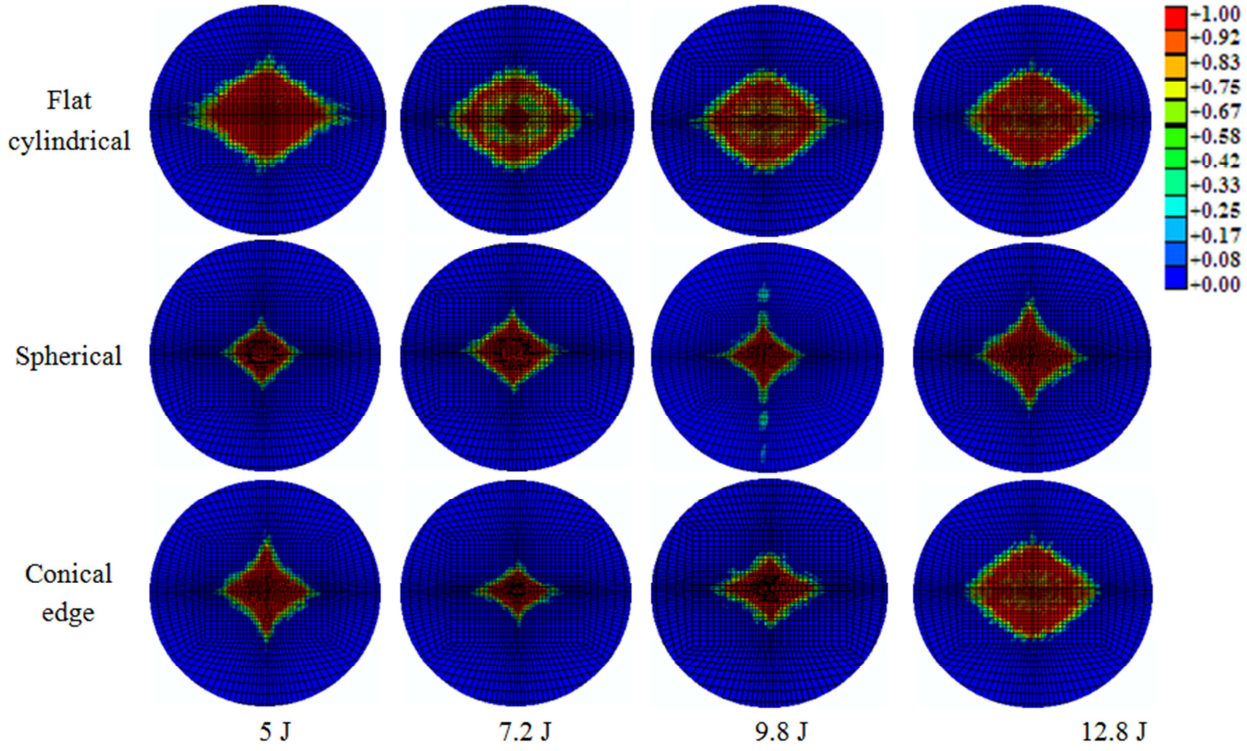

Figure 4. *Delamination area on interface-1 (90/45) for the three impactors under different impact energy levels.*

4.2.2. Comparison of Intra-Laminar Damage with Different Impactors

The variation of intra-laminar damage of selected layers with different impactors under impact energy level of 9.8 J is presented in Figure 6. Result established that damage in the matrix direction is characterized by parallel-shape to the respective angle of ply whiles fiber fracture prediction is represented in longitudinal direction of the fiber. It noted that in the application of the flat cylindrical impactor to activate intra-laminar failure on the composite laminate, an almost circular-shaped pattern is formed. It can be seen that the damage area on the 10th layer is not only massive but with a concentrated damage outlook compared to dotted shape prediction on the 2nd, 4th and 6th layers. Result however, noted a mixed mode of shapes via the spherical ball impactor with largest damage prediction in transverse direction on the 10th layer followed with layers-2, 4 and 6 in descending mode of damage magnitude. Likewise, via the conical shaped impactor to trigger intra-laminar damage on the representative interfaces, varied damage shapes of *asteroid, bat-shaped and spider-shaped patterns* are predicted. With this impactors (conical shaped), least and largest matrix cracking is observed on 6th and 2nd interfaces, respectively. As somewhat perceived, damage areas on the composite laminate correspond to matrix tension, matrix compression, fiber tension and fiber compression as well as fiber-matrix debonding which may perhaps cause by flexural vibration and natural frequency of the impactors. However, only matrix cracking is envisioned to occur due to the low level of energy threshold under this loading condition. Among the layers, the largest matrix cracking occurs on the bottom layer and may arise due to elastic deformation at the interaction area via the flat cylindrical impactor as affirmed in literature [43].

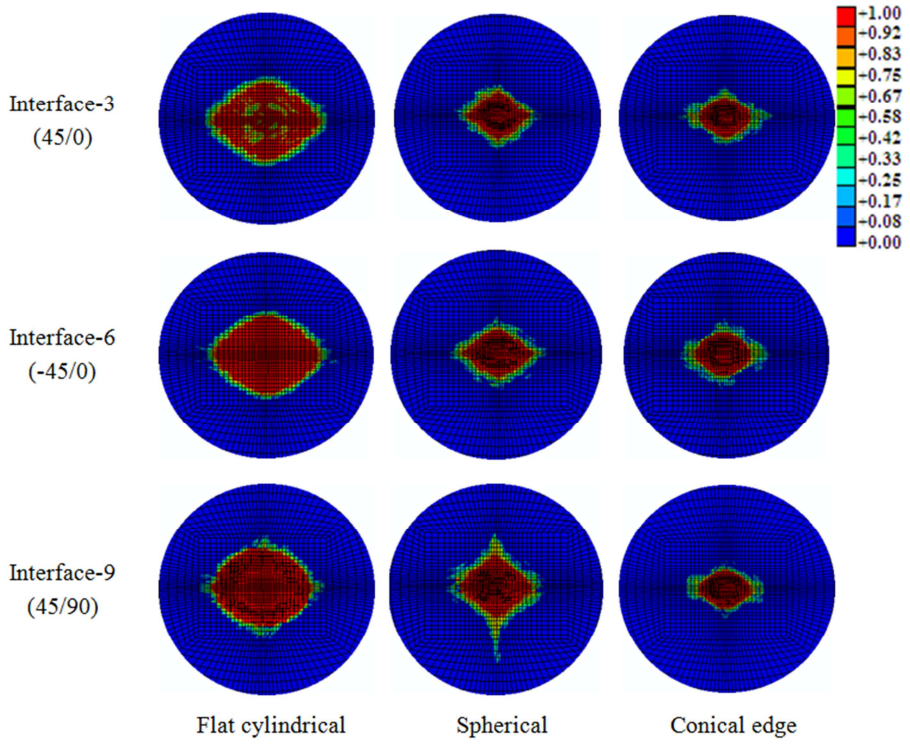

Figure 5. *Delamination profile for selected interfaces with different impactors under impact energy of 7.2J.*

Although, out of plane compression, matrix damage occurs in the transverse direction during damage initiation, yet in-plane matrix tension damage is activated as a result of inter-laminar damage on the last layer. Result also recognized that matrix cracking orients in accordance with fiber direction, which is in better accord with Ref. [42]. The discrepancy between the layers damage areas is significant, and once again, may be attributed to substantial elastic deformation of the composite laminate which leads to induced damage. The figures 5 and 6 indicate that delamination is the largest failure mode in the composite laminate under low velocity impact. Therefore, more consideration is needed in the failure mode analysis due to the great consequences on the compressive strength after impact. Similarly, the delamination area on the bottom layer is bigger than the impact layer of the reinforced S-glass/epoxy composite laminate, and that delamination area shows *spider-shaped* appearance.

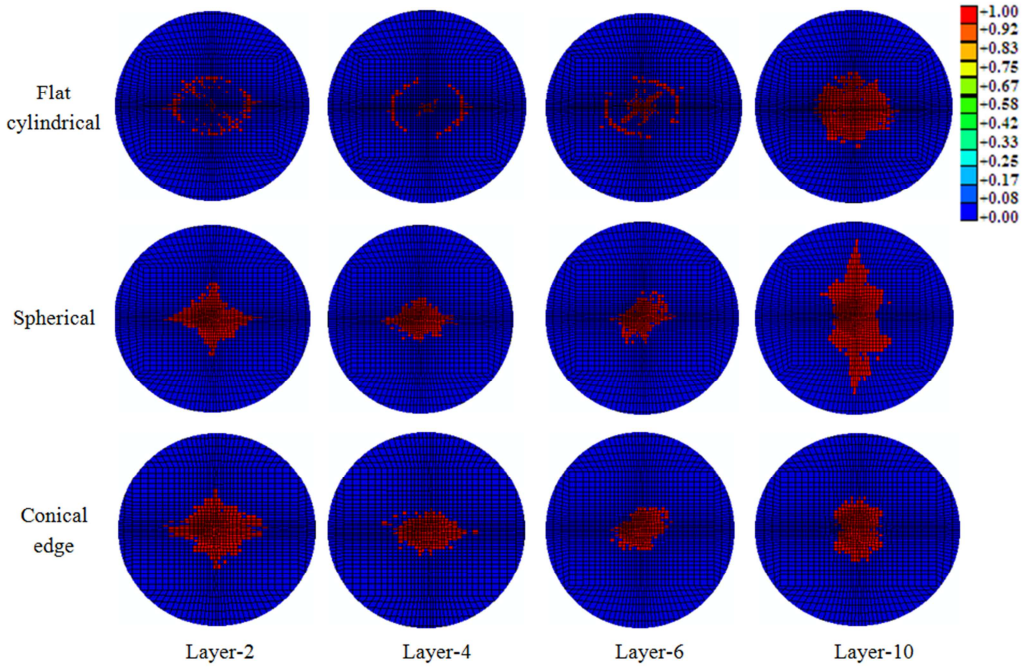

Figure 6. *Comparison of matrix cracking for selected layers with different impactors under impact energy of 9.8 J.*

4.2.3. Comparison of Stress Distribution with Different Impactors

Stress growth and propagation on reinforced composite laminate with different impactors under impact energy threshold of 12.8 J is presented in Figure 7 for evaluation and comparison, and as portrayed, red element on the laminate corresponds to area where failure is anticipated. The stress contour clearly exhibited that the impactor geometry corresponds to yield growth on the reinforced composite lamiante. This is evident via the flat cylindrical and spherical impactors where massive damages are predicted on the 9th layer, followed with 7th and 5th layers with the 1st layer predicting least failure growth. On the other hand, stress distribution on the 1st layer is predicted highest than the 9th layer through the conical edge impactor event. Again in Figure 7, comparing the yield strength under the impact energy regime, its noted that stress distribution on layer-1 of the conical edge impactor is higher than the other two impactors. Similarly, energy distortion on layer-9 is greatest with respect to spherical impactor compared to the other two. Results also revealed that in all the layers irrespective of impactor nose profile, stress pattern of *spider-shaped* is numerically formed. This shows to the fact that both layers oriented parallel to fiber direction, which is believed to have great influence on the extent of damage development.

On the average as acknowledged from the yield stress diagrams, the conical nose impactor predicted the highest stress envelop on the 1st layer with the least captured by the flat headed impactor. Inversely, the flat cylindrical impactor recorded the maximum stress on the 9th layer; hitherto, conical edge impactor projected the least stress. The stress inconsistencies could be ascribed to the geometrical shape of the impactors, and as stated earlier in this segment, stress values correspond to the contact area on the composite laminate. This presupposes that smaller the contact area, the bigger the stress failure formation. Even though, stress regime on the 1st layer is high, the 9th layer could withstand excessive loads resulting in low stress threshold, which is endorsed by the conical nose impactor among the rest. The stress sensation attested to the fact that when impact duration increases, low flexural deformation transpires leading to transverse shear stress which triggers matrix cracking and delamination on the composite lamiante.

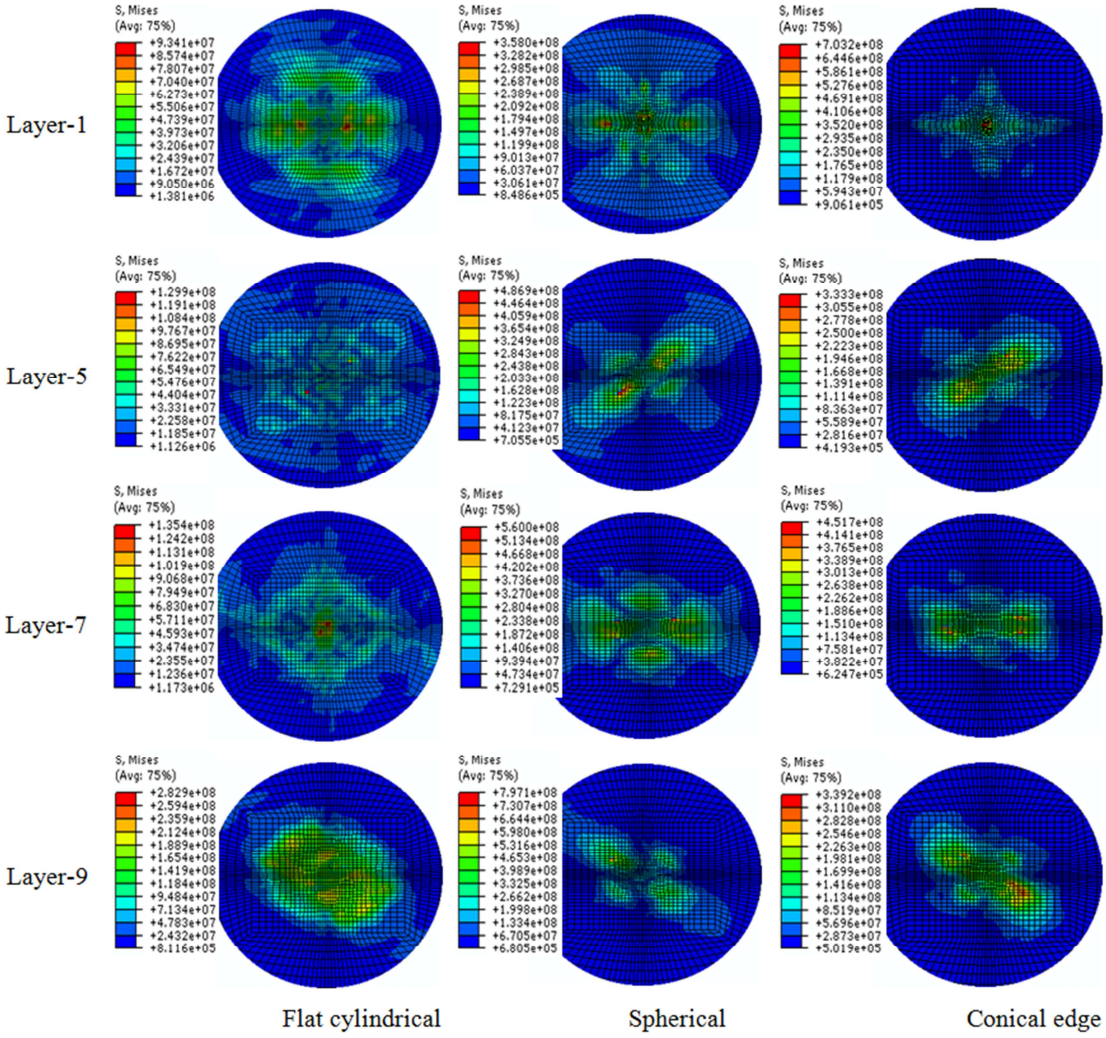

Figure 7. *Von mises stress propagation for typical layers with different impactors under impact energy level of 12.8 J.*

5. Conclusions

This study assesses the structural performance of reinforced S-glass composite laminate at low velocity impact loading with different impactors. Experimental C-scan images were used to validate the model under different impact regimes. A total of 12 samples predictions were performed using three distinct impactors at four different impact energy thresholds.

The last half segment describes the parametric studies to predict the impact behavior on the composite laminate with different impactors. Herein again, analysis was performed to predict intra-laminar, inter-laminar and stress failure responses on the composite laminates with respect to impactor geometry. The model provided an accurate impact prediction at different impact energy levels to characterize the structural behavior for the composite laminates. The following observations were made: (i) damage created via the flat headed impactor was the largest among the impactors showing the effect of impactor geometry. This presupposed that smaller the contact area, the bigger the stress failure formation, and that damage area correspond to contact area on the composite laminate. (ii) irrespective of impactor's profile, stress pattern of spider-shaped was numerically formed on the layers. This attested to the fact that all damage envelops oriented parallel to fiber direction, which was believed to have had great influence on the extent of damage development. (iii) amongst the typical layers, the largest matrix cracking occurs on the bottom layer as a result of major elastic deformation on the interaction area. Again, this damage phenomenon could be attributed to long contact duration between the impactor and bottom layer resulting in transverse shear stresses leading to delamination. Numerical predictions were in reasonable accord with experimental data to substantiate the efficiency and dependability of the developed model under low velocity impact loading conditions. This model is expected to extend to complex structures like aircraft empennage and wing under larger impact threshold where intra-and-inter damage failure is envisioned to occur. As failure in composite materials cannot be eliminated, it is significant to adopt and adapt this model for establishing domains on different structural components to predict damage initiation, progression, energy absorption as well as ultimate impact failures. This study has broadly deepens understanding of engineers and researchers to improve and optimize the design processes of composite materials used in the automobile and aviation structural applications.

Acknowledgements

The research is partially supported by the Innovative Foundation for Doctoral Candidate of Jiangsu Province, China (KYLX15_1049) and the Postdoctoral Science Foundation of Jiangsu Province, China (1402101C) during the course of this work.

References

[1] Artero-Guerrero JA, Pernas-Sánchez J, López-Puente J, Varas D. Experimental study of the impactor mass effect on the low velocity impact of carbon/epoxy woven laminates. Composite Structures. 2015; 133: 774-81.

[2] Panettieri E, Fanteria D, Firrincieli A. Damage initialization techniques for non-sequential FE propagation analysis of delaminations in composite aerospace structures. Meccanica. 2015; 50: 2569-85.

[3] Fanteria D, Panettieri E. A non-linear model for in-plane shear damage and failure of composite laminates. Aerotecnica Missili & Spazio. 2016; 93: 17-24.

[4] Remacha M, Sánchez-Sáez S, López-Romano B, Barbero E. A new device for determining the compression after impact strength in thin laminates. Composite Structures. 2015; 127: 99-107.

[5] Nardi D, Lampani L, Pasquali M, Gaudenzi P. Detection of low-velocity impact-induced delaminations in composite laminates using Auto-Regressive models. Composite Structures. 2016; 151: 108-13.

[6] Drosopoulos GA, Wriggers P, Stavroulakis GE. A multi-scale computational method including contact for the analysis of damage in composite materials. Computational Materials Science. 2014; 95: 522-35.

[7] Evci C. Thickness-dependent energy dissipation characteristics of laminated composites subjected to low velocity impact. Composite Structures. 2015; 133: 508-21.

[8] Guillaud N, Froustey C, Dau F, Viot P. Impact response of thick composite plates under uniaxial tensile preloading. Composite Structures. 2015; 121: 172-81.

[9] Olsson R. Analytical prediction of damage due to large mass impact on thin ply composites. Composites Part A: Applied Science and Manufacturing. 2015; 72: 184-91.

[10] Salvetti M, Gilioli A, Sbarufatti C, Dragan K, Chalimoniuk M, Manes A, et al. Analytical Model to Describe Damage in CFRP Specimen When Subjected to Low Velocity Impacts. Procedia Engineering. 2016; 167: 2-9.

[11] Ahmad F, Hong J-W, Choi HS, Park MK. Hygro effects on the low-velocity impact behavior of unidirectional CFRP composite plates for aircraft applications. Composite Structures. 2016; 135: 276-85.

[12] Farooq U, Myler P. Efficient computational modelling of carbon fibre reinforced laminated composite panels subjected to low velocity drop-weight impact. Materials & Design (1980-2015). 2014; 54: 43-56.

[13] LONGO G. Models and methods to simulate low-energy impact damage on composite aerospace structures. 2011.

[14] Panettieri E, Fanteria D, Danzi F. Delaminations growth in compression after impact test simulations: Influence of cohesive elements parameters on numerical results. Composite Structures. 2016; 137: 140-7.

[15] Fan J, Guan Z, Cantwell WJ. Modeling perforation in glass fiber reinforced composites subjected to low velocity impact loading. Polymer Composites. 2011; 32: 1380-8.

[16] Farooq U, Myler P. Finite element simulation of carbon fibre-reinforced composite laminates subjected to low velocity impact using damage induced static load-deflection methodology. Thin-Walled Structures. 2015; 97: 63-73.

[17] Evci C, Gülgeç M. An experimental investigation on the impact response of composite materials. International Journal of Impact Engineering. 2012; 43: 40-51.

[18] Yang L, Wu Z, Gao D, Liu X. Microscopic damage mechanisms of fibre reinforced composite laminates subjected to low velocity impact. Computational Materials Science. 2016; 111: 148-56.

[19] Panettieri E, Fanteria D, Montemurro M, Froustey C. Low-velocity impact tests on carbon/epoxy composite laminates: A benchmark study. Composites Part B: Engineering. 2016; 107: 9-21.

[20] Mishra A, Naik N. Failure initiation in composite structures under low-velocity impact: Analytical studies. Composite Structures. 2010; 92: 436-44.

[21] Lopresto V, Caprino G. Damage mechanisms and energy absorption in composite laminates under low velocity impact loads. Dynamic Failure of Composite and Sandwich Structures: Springer; 2013. p. 209-89.

[22] Singh H, Mahajan P. Analytical modeling of low velocity large mass impact on composite plate including damage evolution. Composite Structures. 2016; 149: 79-92.

[23] Farooq U, Myler P. Finite element simulation of damage and failure predictions of relatively thick carbon fibre-reinforced laminated composite panels subjected to flat and round noses low velocity drop-weight impact. Thin-Walled Structures. 2016; 104: 82-105.

[24] Topac OT, Gozluklu B, Gurses E, Coker D. Experimental and computational study of the damage process in CFRP composite beams under low-velocity impact. Composites Part A: Applied Science and Manufacturing. 2017; 92: 167-82.

[25] Sakly A, Laksimi A, Kebir H, Benmedakhen S. Experimental and modelling study of low velocity impacts on composite sandwich structures for railway applications. Engineering Failure Analysis. 2016; 68: 22-31.

[26] Lopes C, Sádaba S, González C, Llorca J, Camanho P. Physically-sound simulation of low-velocity impact on fiber reinforced laminates. International Journal of Impact Engineering. 2016; 92: 3-17.

[27] Pérez MA, Martínez X, Oller S, Gil L, Rastellini F, Flores F. Impact damage prediction in carbon fiber-reinforced laminated composite using the matrix-reinforced mixing theory. Composite Structures. 2013; 104: 239-48.

[28] Alshahrani RF, Merah N, Khan SM, Al-Nassar Y. On the impact-induced damage in glass fiber reinforced epoxy pipes. International Journal of Impact Engineering. 2016; 97: 57-65.

[29] Bienias J, Jakubczak P, Dadej K. Low-velocity impact resistance of aluminium glass laminates–Experimental and numerical investigation. Composite Structures. 2016; 152: 339-48.

[30] Duodu EA, Gu J, Ding W, Shang Z, Tang SJIJoS, Technology ToME. Simulation of composite laminate with cohesive interface elements under low-velocity impact loading. 2019; 43: 127-38.

[31] Maio L, Monaco E, Ricci F, Lecce L. Simulation of low velocity impact on composite laminates with progressive failure analysis. Composite Structures. 2013; 103: 75-85.

[32] Farooq U, Myler P. Flat nose low velocity drop-weight impact response of carbon bre composites using non-destructive damage detection techniques. 2015.

[33] Farooq U. Finite element simulation of flat nose low velocity impact behaviour of carbon fibre composite laminates: University of Bolton; 2014.

[34] Whisler D, Kim H. Effect of impactor radius on low-velocity impact damage of glass/epoxy composites. Journal of Composite Materials. 2012; 46: 3137-49.

[35] Sepe R, De Luca A, Lamanna G, Caputo F. Numerical and experimental investigation of residual strength of a LVI damaged CFRP omega stiffened panel with a cut-out. Composites Part B: Engineering. 2016; 102: 38-56.

[36] Long S, Yao X, Zhang X. Delamination prediction in composite laminates under low-velocity impact. Composite Structures. 2015; 132: 290-8.

[37] Version A. 6.11. User's manual. Dassault Systemes. 2011.

[38] Manual AUs. Version 6.11. ABAQUS Inc: Providence, RI, USA. 2011.

[39] Bandaru AK, Ahmad S. Modeling of progressive damage for composites under ballistic impact. Composites Part B: Engineering. 2016; 93: 75-87.

[40] Shi Y, Swait T, Soutis C. Modelling damage evolution in composite laminates subjected to low velocity impact. Composite Structures. 2012; 94: 2902-13.

[41] Zarei H, Sadighi M, Minak G. Ballistic analysis of fiber metal laminates impacted by flat and conical impactors. Composite Structures. 2017; 161: 65-72.

[42] Yang L, Yan Y, Kuang N. Experimental and numerical investigation of aramid fibre reinforced laminates subjected to low velocity impact. Polymer Testing. 2013; 32: 1163-73.

[43] Ansari MM, Chakrabarti A. Influence of projectile nose shape and incidence angle on the ballistic perforation of laminated glass fiber composite plate. Composites Science and Technology. 2017; 142: 107-16.